Unhindered Biplane-Shaped N-Heterocyclic Carbene Ligands as a Remedy for Low Reactivity of Crowded Substrates in Ruthenium Catalyzed Olefin Metathesis

Pawel Krzesiński, Chiara Dinoi, Iker Del rosal, Laure Vendier, Stéphanie Bastin, Vincent César, Anna Kajetanowicz, Karol Grela

Unhindered Biplane-Shaped N-Heterocyclic Carbene Ligands as a Remedy for Low Reactivity of Crowded Substrates in Ruthenium Catalyzed Olefin Metathesis

Paweł Krzesiński,[a,b] Chiara Dinoi,[c] Iker del Rosal,[c] Laure Vendier,[b] Stéphanie Bastin,[b,*] Vincent César,[b,*] Anna Kajetanowicz,[a,*] Karol Grela[a,*]

[a] Biological and Chemical Research Centre, Faculty of Chemistry, University of Warsaw, Żwirki i Wigury 101, 02-089 Warsaw, Poland
[b] LCC-CNRS, Université de Toulouse, CNRS, 205 route de Narbonne, 31077 Toulouse cedex 4, France
[c] LPCNO, Université de Toulouse, INSA Toulouse, CNRS, UPS, 135 Avenue de Rangueil, 31077 Toulouse, France.

Keywords: Olefin Metathesis, Ruthenium Catalysts, N-Heterocyclic Carbene, Catalyst Design, Tetrasubstituted Double Bond Formation

Abstract: Despite notable progress, olefin metathesis methods for preparing sterically crowded C-C double bonds remain scarce. They are commonly based on specialized ruthenium catalysts with sterically reduced N-heterocyclic carbene (NHC) ligands, able to accommodate more crowded olefinic substrates during the catalytic steps. Yet, although being highly active, these complexes are rather unstable, mainly due to intramolecular C-H activation at the *ortho* position of an *N*-aryl group of the NHC ligand, leading to catalyst deactivation. Considering that the deleterious C-H activation process requires the rotation of the *N*-aryl arm of the NHC ligand, we introduced a second decker of aromatic groups in benzimidazolylidene-based *N*-phenyl NHC ligands, which leads to robust and highly efficient ruthenium metathesis catalysts in challenging metathesis reactions of tri-and tetra-substituted olefins. The beneficial effect of these upper aromatic "wings" on the stability and activity of the Ru-complexes is rationalized through the experimental determination of the stereoelectronic properties of the NHC ligands, complemented by DFT calculations on the nature of the through-space interactions between the aromatics and on the decomposition pathway of the second-generation Hoveyda precursors.

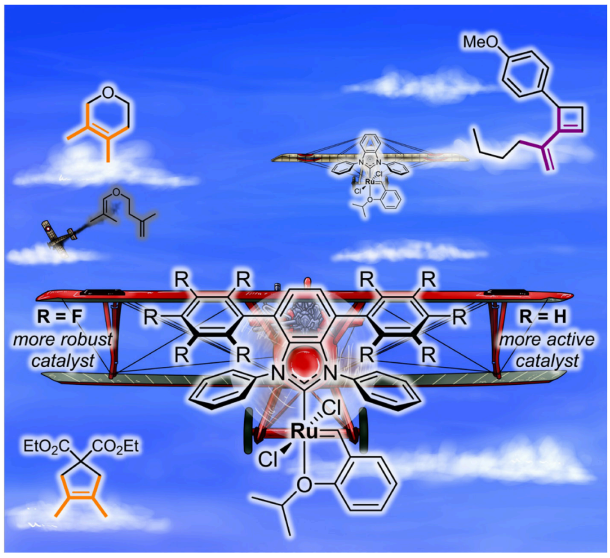

INTRODUCTION

Olefin metathesis has become a device of prominent importance for C–C double bond formation thus earning an outstanding position in the organic synthesis toolbox.[1-4] Especially well-defined ruthenium-based alkylidene complexes are widely used as catalysts due to their stability towards air and moisture. The discovery of N-heterocyclic carbenes (NHCs)[5-10] has made a great impact in the field giving birth to even more stable and efficient second generation catalysts (e.g. **Ru1** and **Ru2**, Figure 1).[11,12]

Despite the incredible progress made in the discipline, there are still many hurdles to overcome, one of which is the ineffectiveness of these popular, general-purpose ruthenium catalysts in the formation of tetrasubstituted or crowded C–C double bonds (Figure 1).[13,14,15]

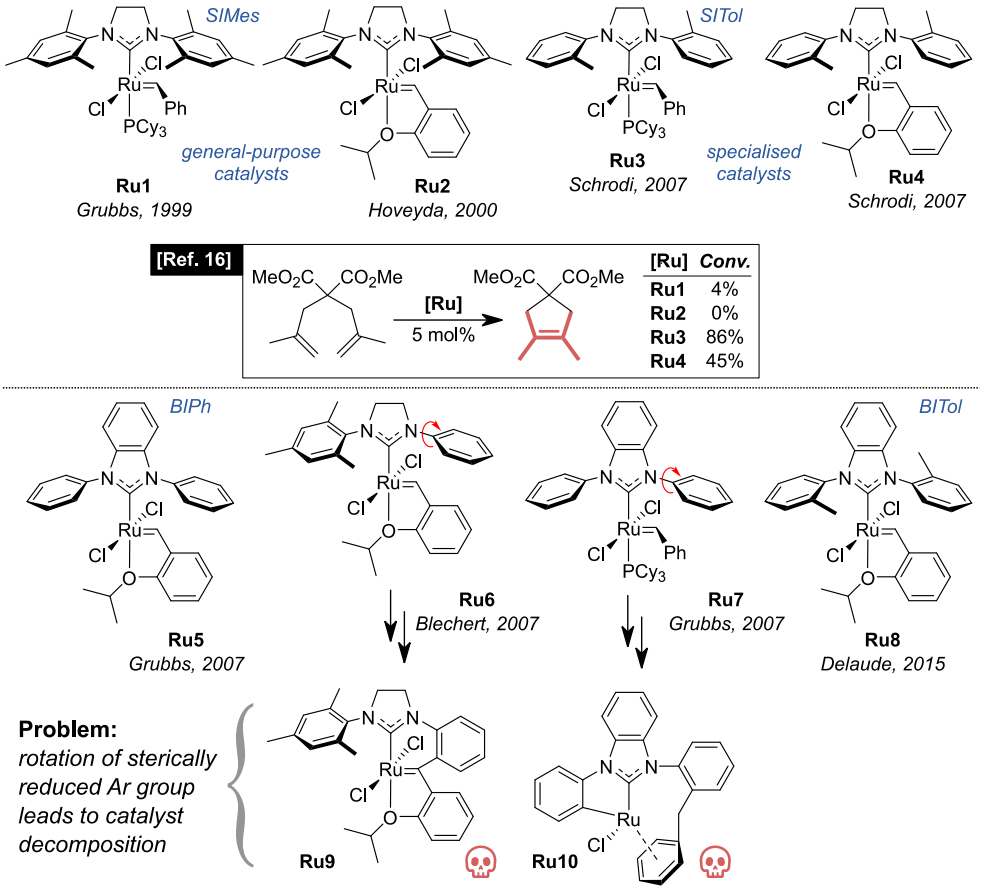

Figure 1. Selected general-purpose catalysts (**Ru1**, **Ru2**) versus sterically reduced ones (**Ru3**–**Ru8**) designed for the formation of tetrasubstituted C–C double bonds, and associated decomposition products (**Ru9**, **Ru10**). In the inset is shown an example of a challenging metathesis reaction.[16]

In 2007, Grubbs and Schrodi reported a practical solution to this essential problem by developing a series of ruthenium catalysts bearing NHC ligands with sterically less hindered, mono-*ortho* substituted *N*-aryl groups (**Ru3** and **Ru4**, Figure 1).[16,17] The proposed explanation for their higher activity is fairly straightforward and widely accepted—the smaller demand of the "chopped" NHC

ligand allows for more facile coordination of sterically crowded olefins to the ruthenium metal center.[18] About the same time, other structures were developed (e.g. **Ru5** – **Ru7**, Figure 1) based on the same concept.[17,19,20,21,22]

Although these new catalysts are more efficient in the formation of crowded and tetrasubstituted olefins than popular general purpose complexes, such as **Ru1** and **Ru2**, it was quickly observed that they strongly suffer from decreased stability and increased sensitivity to air and other poisons.[19,23] Blechert *et al.* investigated the mechanism of deactivation of **Ru6**, which consisted of sequential pericyclic cyclization, oxidation, and elimination steps yielding the metathesis-inactive product **Ru9** (Figure 1).[19] Particularly, when both arms of the NHC ligand are sterically reduced, the resulting catalyst (e.g. **Ru7**) is extremely prone to deactivation, following pathways including C-H activation in *ortho N*-phenyl position, which after insertion in alkylidene gives the permanently deactivated complex **Ru10** (Figure 1).[23-25]

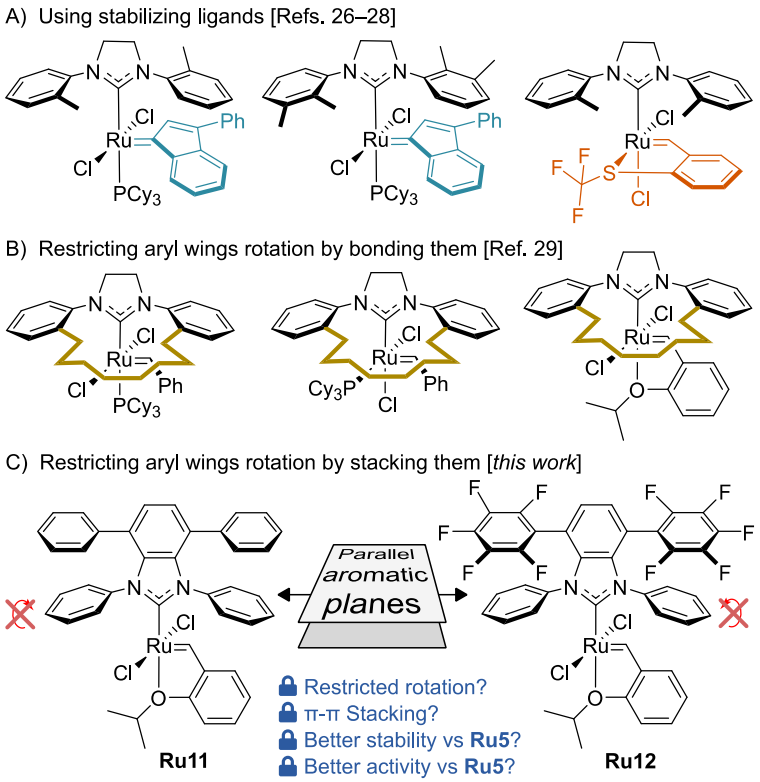

Figure 2. Selected approaches to stabilize small-NHC ruthenium catalysts, A) by using stabilizing ligands, B, C) by restricting aryl ring rotation.[26-28,29]

The instability of ruthenium complexes induced by the use of low sterically hindered NHC ligands can be mitigated to some extent by using indenylidene[26,27] or thioether benzylidene ligands that are known to increase the thermodynamic stability of Ru catalysts (Figure 2A).[28] It is clear that the initial step in catalyst decomposition is the rotation of the *N*-aryl until which is coplanar with the imidazolidinylidene ring,[30] therefore some effort has been put into the synthesis of NHC-based Ru complexes with restricted *N*-aryl rotation while maintaining the low steric demand of the NHC

ligand.[30-32] Our group has recently published an example how such an approach can deliver enhanced catalyst stability and productivity (Figure 2B). [29]

Perhaps due to their limited applications, benzimidazolylidene ruthenium catalysts did not gain much interest. Delaude and co-workers reported, in their scholarly work, the synthesis of ruthenium catalysts having benzimidazolylidene NHC ligand with *ortho*-tolyl (**Ru7**, Figure 1) and mesityl *N*-substituents.[33,34] We reasoned that such a ligand architecture would be ideal for the installation of a second decker of aromatic rings, which would hinder the *N*-aryl rings' rotation. According to this working hypothesis, catalysts **Ru11** and **Ru12** (Figure 2C), featuring the smallest possible set of aryl *N*-substituents at the NHC ligand, *i.e.* phenyl groups, may display higher stability than their parent complex **Ru5**, while their activity in the challenging metathesis of sterically crowded bonds would be maintained and, hopefully, even enhanced. Electronically-different phenyl (in **Ru11**) and pentafluorophenyl (in **Ru12**) groups were chosen as second-decker aryl groups to investigate the possible peculiarities of these hitherto unknown architectures, such as a potential presence of π-π interactions and modulated electronic properties.

RESULTS

Synthesis of NHC precursors. Commercially available 4,7-dibromo-2,1,3-benzothiadiazole (**1**) was chosen as a precursor for both phenyl and pentafluorophenyl substituted benzimidazolium salts **5** and **8** (Scheme 1). Suzuki coupling allowed for the installation of phenyl groups in the backbone motif, while subsequent reductive sulfur extrusion gave access to *o*-phenylenediamine derivative **2** in 72% yield over two steps. Next, the bicyclic benzimidazole skeleton was obtained using a standard cyclization protocol with triethyl orthoformate, affording **3** in quantitative yield. Products **2** and **3** were obtained on a gram scale without purification by column chromatography. In the final step, the desired benzimidazolium salt **5** was obtained using copper-catalyzed arylation with diphenyliodonium tetrafluoroborate.[35] Worth highlighting is that such direct arylation of NH imidazole to imidazolium salt has never been reported in the literature.[35-37] This protocol gave a mixture of the desired *N,N'*-diphenylbenzimidazolium salt **5** (36% isolated yield) and neutral *N*-phenylbenzimidazole **4** (58% isolated yield) which were separated using column chromatography. The succeeding arylation of isolated **4** gave salt **5** in 77% yield, therefore the two subsequent arylation reactions lead to compound **5** in an 81% overall yield.

Synthesis of pentafluorophenyl substituted derivative **8** turned out to be a more synthetic challenge (see Supporting Information for experimental details on pre-ligands synthesis). A Kumada-Corriu coupling was successfully employed to graft pentafluorophenyl groups into the benzothiadiazole motif. The subsequent reductive sulfur extrusion step gave *o*-phenylenediamine derivative **6** in 55% yield over the two steps. Unlike the synthesis of salt **5**, the *N*-phenyl groups were first installed

through a Buchwald-Hartwig amination, giving compound **7** in 21% isolated yield. In a final step, the benzimidazolium salt **8** was obtained with quantitative yield using a modified cyclization protocol using triethyl orthoformate in the presence of $HBF_4 \times Et_2O$.

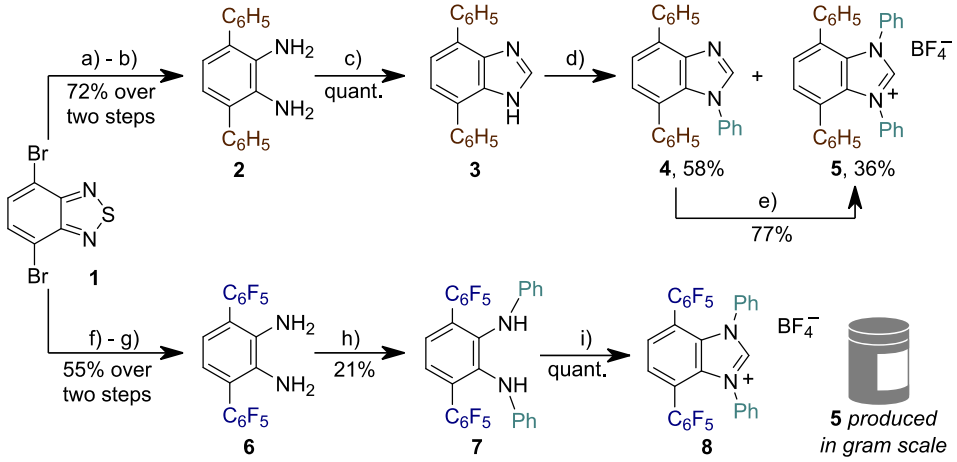

Scheme 1. Synthesis of benzimidazolium salts **5** and **8**. Reaction conditions: a) 2.1 equiv. $PhB(OH)_2$, 4 equiv. K_2CO_3, 0.8 mol% $Pd(PPh_3)_4$, toluene/water 2.5 : 1 v/v, reflux, overnight; b) 9 equiv. $NaBH_4$, 6 mol% $CoCl_2 \times 6H_2O$, EtOH/THF 3:1 v/v, reflux, 3 h; c) $(EtO)_3CH$ (excess), 6 equiv. HCl_{aq}, reflux, overnight; d) 2 × 2 equiv. Ph_2IBF_4, 2 × 5 mol% $Cu(OAc)_2 \times H_2O$, DMF, 100 °C, 24 h, then 48 h; e) 2 equiv. Ph_2IBF_4, 7.5 mol% $Cu(OAc)_2 \times H_2O$, DMF, 100 °C, overnight; f) 3 equiv. $BrMgC_6F_5$, 10 mol% $Pd(PPh_3)_3$, THF, 70 °C, overnight; g) 3 equiv. $NaBH_4$, 7 mol% $CoCl_2 \times 6H_2O$, EtOH/THF 3:1 v/v, 50 °C, 5 min.; h) PhBr (excess), 2.5 mol% $Pd_2(dba)_3$, 7.5 mol% P^tBu_3, 1.5 equiv. KHMDS, 160 °C, 30 min.; i) $(EtO)_3CH$ (excess), 1 equiv. $HBF_4 \times Et_2O$, 60 °C, 30 min.

Synthesis of ruthenium catalysts. The corresponding Hoveyda-Grubbs complexes were obtained by displacement of the tricyclohexylphosphine ligand in ruthenium precursor **Ru13** by the free NHCs generated using $KOC(CF_3)CH_3$ as a base (Scheme 2A). Complex **Ru12** was isolated using column chromatography, whereas complex **Ru11** was purified by simple crystallization from a tetrahydrofuran-pentane mixture. Both complexes (brown-orange solids) are stable for months when stored in a protective atmosphere. It is noteworthy that upon the synthesis of known **Ru5** (see Supporting Information for details),[17] we noticed its fragility when column chromatography was performed with regular solvents. Even with carefully degassed dry solvents, complex **Ru5** was obtained in only 19% yield, which is considerably lower than in the case of **Ru11** and **Ru12**, 72% and 43% respectively. The molecular structures of complexes **Ru11** and **Ru12** were confirmed by X-ray diffraction experiments on single crystals grown by layering dichloromethane complex solutions of **Ru11** and **Ru12** with pentane (respectively, Scheme 2B and C, Figure 3, Table 2, and Supporting Information for details).

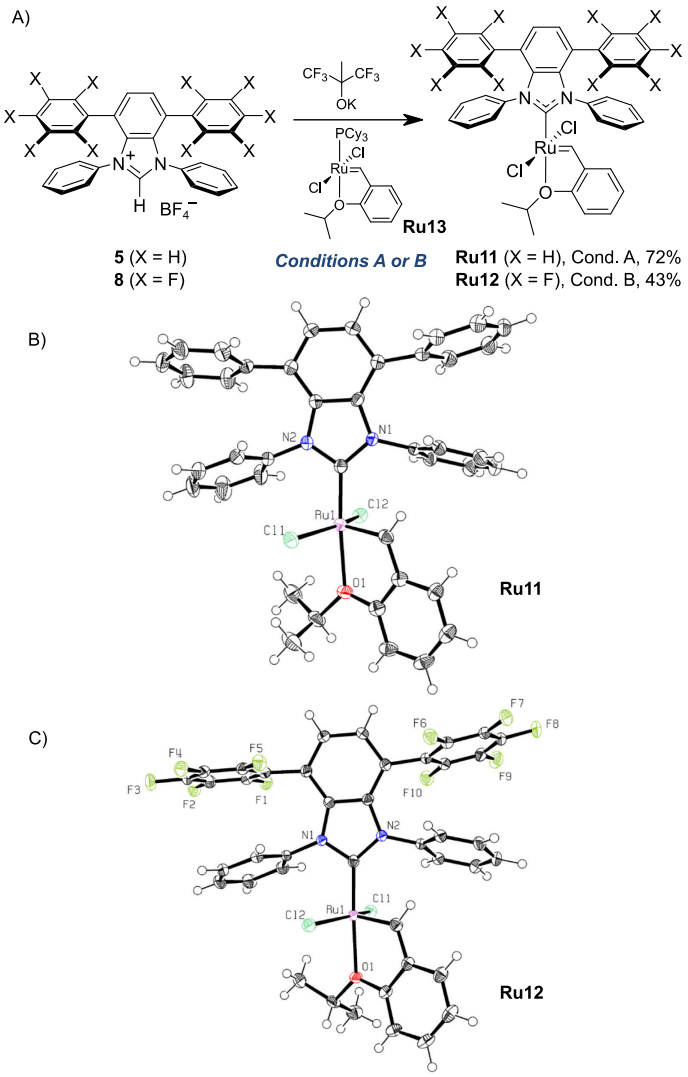

Scheme 2. A) Synthesis of **Ru11** and **Ru12**; conditions A: *i*) 1.75 equiv. of **5**, 1.75 equiv. $KOC(CF_3)CH_3$, benzene, rt, 30 min., *ii*) 1 equiv. **Ru13**, 60 °C, 1 h; conditions B: *i*) 1.75 equiv. of **8**, 2 equiv. $KOC(CF_3)CH_3$, benzene, rt, 15 min., *ii*) 1 equiv. **Ru13**, 60 °C, 30 min. B) XRD structure of **Ru11**, ellipsoids are drawn at 50% probability. C) XRD structure of **Ru12**, ellipsoids are drawn at 50% probability.

Evaluation of electronic and steric properties of new NHC ligands and catalysts. An in-depth characterization of the electronic properties of the three ligands was then carried out (Scheme 3 and Table 1). The overall electron-donating ability of the NHC ligands was first quantified by recording the average stretching frequency, ν_{CO}^{av}, of the carbonyl ligands in complexes **Rh1**-**Rh3**, which is correlated to the Tolman Electronic Parameter (TEP) value of the ligand by a well-established linear correlation.[10] Additionally, the σ-donating and the π-accepting abilities of the NHCs can be independently assessed by measuring the $^1\mathcal{J}_{CH}$ coupling constant between the carbon and the hydrogen atoms on the pre-carbenic position in the azolium precursors and by recording the chemical shift of ^{77}Se nuclei in the seleno adducts **Se1**-**Se3** respectively.[38] The experimental data first confirmed that the three benzimidazole-based NHCs are less donating than their imidazol(in)e-based congeners **IMes** and **SIMes**. Within the benzimidazolylidene series, the presence of the two

distal phenyl groups in **BI*Ph**[39] slightly increased its σ-donation but also its π-acidity relative to the unsubstituted **BIPh**, leading to a slightly stronger overall electronic donation with a TEP value of 2052.2 cm^{-1}. In contrast, perfluorination of the backbone-aryl groups induced a noticeable decrease in electronic donation with a TEP value ranging from 2052.2 cm^{-1} for **BI*Ph** to 2056.2 cm^{-1} for **BIF*Ph**, as could be anticipated in view of the strong electron-withdrawing effect of fluorine atoms. Overall, starting from the unsubstituted **BIPh**, the installation of the second aryl layer at the rear of the benzimidazolyl core generates the more electron-donating **BI*Ph** ligand and the less electron-donating **BIF*Ph** ligands.

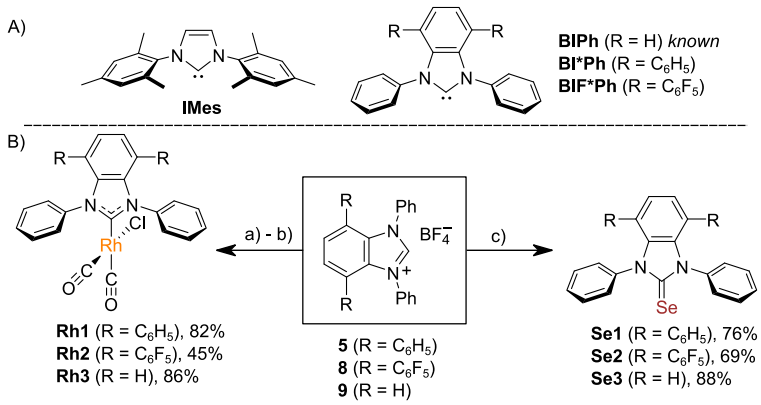

Scheme 3. A) Structures and abbreviations of NHC ligands studied herewith. B) Synthesis of rhodium carbonyl complexes and selenium adducts. Reaction conditions: a) *i*) 2.2 equiv. of benzimidazolium precursor, 2.2 equiv. $KOC(CF_3)_2CH_3$, THF, rt, 30 min., *ii*) 1 equiv. $[RhCl(COD)]_2$, overnight; b) CO (excess), DCM, rt, 30 min.; c) *i*) 1 equiv. of benzimidazolium precursor, 1 equiv. $KOC(CF_3)_2CH_3$, THF, rt, 30 min., *ii*) 2 equiv. Se, overnight.

Table 1. Measured stereoelectronic parameters of **SIMes**, **IMes**, **BIPh**, **BI*Ph** and **BIF*Ph**

Ligand	νCO^{av}[a] [cm^{-1}]	TEP value[b] [cm^{-1}]	$^1J_{CH}$ [40]	$\delta(^{77}Se)$[c] [ppm]	$\%V_{bur}$ [%][d]
SIMes	*lit. 2037.5*[e]	2050.2	*lit. 206*[f]	*lit. 110*[g]	33.7[h]
IMes	2037.5 (*lit. 2037.6*)[i]	2050.2 (2050.3)	225 (*lit. 225*)[f]	27 (*lit. 27*)[g]	n.a.[j]
BIPh	2043.0	2054.6	224	127	32.9[k]
BI*Ph	2040.0	2052.2	222	160	31.6
BIF*Ph	2045.0	2056.2	226	198	31.6

[a] Measured in CH_2Cl_2. [b] TEP = (0.8001 × νCO^{av}) + 420.0 cm^{-1}. [c] Measured in $CDCl_3$. [d] Calculated from XRD structures of the corresponding Grubbs-Hoveyda complexes. [e] From ref [41]. [f] From ref [38]. [g] From ref [42]. [h] XRD structure retrieved from ref [43,44] [i] From ref [45]. [j] n.a. = not available; no single crystal XRD structure of **IMes**-derived Grubbs-Hoveyda complex has been reported. [k] XRD structure retrieved from ref [17,46]

Selected bond lengths and angles of complexes **Ru11** and **Ru12** are presented in Table 2, along with

the corresponding ones for the previously reported complex **Ru5**,[17,46] which may serve as the reference compound. The geometrical parameters describing the structures of complexes **Ru11** and **Ru12** correlate well with the one of reference **Ru5**, as illustrated by the superimposed structures (Figure 3B). The lengths of the Ru-C_{NHC} and the Ru=$C_{alkylidene}$ in the three complexes do not differ of more than three estimated standard deviations, as well as the geometry index (τ_5),[47] which characterizes the distortion of the square-pyramidal geometry [**Ru5**: 0.35; **Ru11**: 0.38; **Ru12**: 0.40]. However, Ru-O bond distances significantly increase in order **Ru12**, **Ru5**, **Ru11**, respectively, which perfectly correlates with the NHCs electronic donation abilities (overall and σ-donation) rising in this order **BI*FPh** < **BIPh** < **BI*Ph**, reflecting structural *trans* effect from **BI*FPh** to **BIPh** and to **BI*Ph**.[48] Interestingly, such observation differs from phosphine derived second generation OM catalysts (e.g. **Ru1**) where the increased π-acidity of NHC ligand accounts for stronger *trans* effect as the resulting metal-phosphine π-backdonation weakens.[49] Obviously isopropoxy ligand is a purer σ-donor hence stronger σ-donating NHC will have a stronger *trans* effect. Such a trend can also be observed in other examples in the literature although, to the best of our knowledge, no such assumption has been made so far.[50]

The relative steric constraints of the parent unsubstituted **BIPh** and the two new double-decker **BI*Ph** and **BIF*Ph** ligands were quantified by establishing their topographical steric maps in complexes **Ru5**, **Ru11**, and **Ru12** respectively, using the SambVca2 web application (Figure 3A),[51] and were compared to the steric hindrance brought by the **SIMes** ligand in the general-purpose catalyst **Ru2**.[43,44] Interestingly, it appeared that the substitution of the benzimidazolyl backbone led to a slight decrease of the $\%V_{bur}$ from 32.9% for **BIPh** in **Ru5** to 31.6% for **BI*Ph** and **BIF*Ph** in **Ru11** and **Ru12**, which arises from a higher orthogonality of the *N*-phenyl groups relative to the benzimidazolyl heterocycle, characterized by the increase of the dihedral angles C7-N2-C8-C9 and C2-N1-C10-C11 from 48.21° and 62.91° in **Ru5** to 69.23° and 77.17° in **Ru11** and 77.30° and 66.24° in **Ru12**. This may be ascribed to the substitution of the backbone of the benzimidazolyl ring by phenyl and pentafluorophenyl rings in **Ru11** and **Ru12** respectively, which hinders the *N*-phenyl rotation as hypothesized. This through-space effect of the backbone substitution is the opposite of the buttressing effect observed in amino-decorated NHC catalysts, in which the bulky amino substituents on the backbone forced the *N*-aryl groups to be twisted.[45,52] As expected, all three benzimidazolylidene ligands provide a lower steric pressure than the standard **SIMes** ligand [$\%V_{bur}$(**SIMes**) = 33.7%], due to the presence of small *N*-phenyl groups.

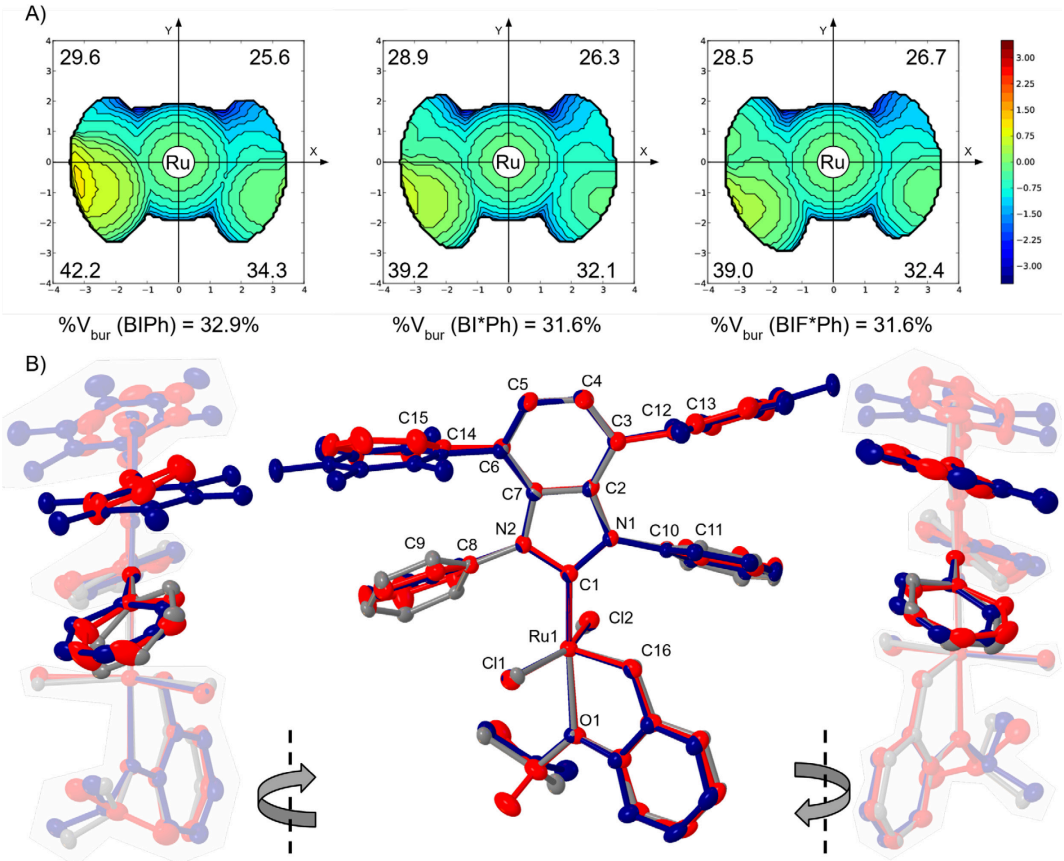

Figure 3. A) Steric maps of NHC ligands in complexes: left—**Ru5**, center— **Ru11**, right— **Ru12**. Values in the four corners of the maps are the %V_{bur} of the NHC ligand in the corresponding quadrant. B) Superimposed structures of **Ru5** (gray), **Ru11** (red) and **Ru12** (blue).

Furthermore, when **Ru11** and **Ru12** are compared, although dihedral angles between the *N*-phenyl groups and the benzimidazolyl ring do not clearly stand out one from another, dihedral angles between NHC core and phenyl or pentafluorophenyl upper deck substituents (angles C2-N1-C10-C11 and C5-C6-C14-C15, respectively) explicitly increase from 62.50°, 63.79° to 70.32°, 79.38°, respectively. This observation could be explained by stronger π-π interactions between the two aromatic planes in the structure of **Ru12**.

Table 2. Selected, corresponding bond lengths (Å) and angles (deg) in X-ray crystal structures of complexes **Ru5**, **Ru11**, and **Ru12**. Atom labeling corresponds to Figure 3B and not to CIF files.

	Ru5[46]	**Ru11**	**Ru12**
Ru1-C1	1.9618(10)	1.968(3)	1.9585(17)
Ru1-C16	1.8365(11)	1.830(3)	1.8326(17)
Ru1-O1	2.2692(7)	2.2807(19)	2.2539(12)
C1-Ru1-O1	176.19(4)	175.61(9)	177.09(5)

Cl1-Ru1-Cl2	155.303(10)	153.04(3)	153.163(14)
C7-N2-C8-C9	48.21	69.23	77.30
C2-N1-C10-C11	62.91	77.17	66.24
C5-C6-C14-C15	-	62.50	79.38
C4-C3-C12-C13	-	63.79	70.32

In order to rationalize the effect of the insertion of a phenyl or pentafluorophenyl ring in the backbone of the benzimidazolyl group of **Ru11** and **Ru12** respectively, we carried out a DFT study at the B3PW91-D3 level of theory. The optimized structure of **Ru11** and **Ru12** (**11opt** and **12opt**, respectively), are shown in Figure S11. Selected bond distances and angles are listed in Table S11 and compared with those experimentally observed. The computed bond distances and angles accurately reproduce the experimental values with variations of less than 0.04 Å. Taking into account the free rotation of both the *N*-phenyl and the benzimidazolyl-phenyl or pentafluorophenyl rings, the disparities observed in the torsion angles between the experimental and computed structures are likely to be attributed to packing interactions within the crystal lattices.

To better characterize the interactions between the *N*-phenyl and the benzimidazolyl-phenyl or pentafluorophenyl rings, the natural charges of complexes **11opt** and **12opt** have been computed by NBO analysis (Figure S12). In complex **11opt**, the carbon atoms of both the *N*-phenyl and benzimidazolyl-phenyl rings display negative charges (in the range −0.235 to −0.249 and −0.227 to −0.250 for the *N*-phenyl and benzimidazolyl-phenyl groups respectively). Conversely, in complex **12opt**, while the carbon atoms of the *N*-phenyl display negative charges (in the range −0.230 to −0.254), those of the pentafluorophenyl rings display positive charges (in the range 0.300 to 0.393). According to the model proposed by Hunter and Sanders,[53] the electron-withdrawing F substituents would reduce the negative quadrupole moment of the second-decker aromatic rings, thereby favoring parallel displaced sandwich conformations in complex **12opt**. In order to check for the possible presence of π-π orbital interactions between the *N*-phenyl and the backbone-phenyl or -pentafluorophenyl rings, we also carried out molecular orbital analysis of compounds **11opt** and **12opt**. As previously suggested,[54] indeed, when two aromatic rings are near enough to each other, their π orbital overlapping may provide an additional binding force to their stacking interaction (Figures S13 and S14). While for complex **11opt**, no π orbital overlapping between the *N*-phenyl and the backbone-phenyl rings is observed, in complex **12opt**, on the other hand, the HOMO-15 orbital displays a small π orbital overlapping between the *N*-phenyl and the backbone-pentafluorophenyl

rings. The analysis of the interaction between the *N*-phenyl and the second decker-phenyl or pentafluorophenyl rings by comparing their different *i*) centroid's distances (3.607 and 3.427 Å for **11opt** and **12opt** respectively), *ii*) quadrupole moments and *iii*) π orbital overlapping suggests therefore that the *N*-phenyl ring interacts more strongly with the backbone-pentafluorophenyl ring in **12opt** than with the backbone-phenyl ring in **11opt**.

Catalysts stability in solution. The stability of the two newly obtained biplane-type NHC ruthenium complexes **Ru11** and **Ru12** was then quantitatively monitored and compared with the benchmark **Ru5**. Since NHC ligand remains coordinated to the metal center throughout the entire catalytic cycle, the differences in complexes' stability should directly translate to the stability of actual propagating species, thus conveying their effectiveness in catalysis. Gratifyingly, **Ru11** and **Ru12** remained perfectly unchanged for approximately three weeks in solution at ambient temperature, while **Ru5** slowly degraded to around 50% of the initial amount (Figure 4A, left). This fact confirmed our previous observation that upon isolation the top-covered complexes **Ru11** and **Ru12** *are considerably more stable* than **Ru5**. Furthermore, the differences in stability were even more pronounced at higher temperature (Figure 4A, right), where **Ru5** disappeared completely after about 27 hours, while **Ru11** and **Ru12** were still detectable even after more than 100 hours in solution at 80 °C. Furthermore, the elevated temperature allowed to distinguish **Ru11** from **Ru12** in terms of stability and **Ru12** proved to be the more stable catalyst, which we assign to the beneficial impact of the π-π interactions between *N*-phenyl groups and phenyl or pentafluorophenyl backbone motifs. To unambiguously confirm the nature of the catalyst deactivation pathway, we attempted to isolate the degradation product of **Ru5**.[23,55] After stirring **Ru5** in dichloromethane at 40 °C for one week, the expected, tethered η^6-arene-NHC Ru(II) complex **Ru14** was isolated (Figure 4B), whose formation should proceed through the activation of an *ortho* C-H bond of one *N*-phenyl group followed by alkylidene insertion. The molecular structures of complex **Ru14** was confirmed by X-ray diffraction experiments on single crystals grown by layering dichloromethane complex solution with pentane (Figure 4C).

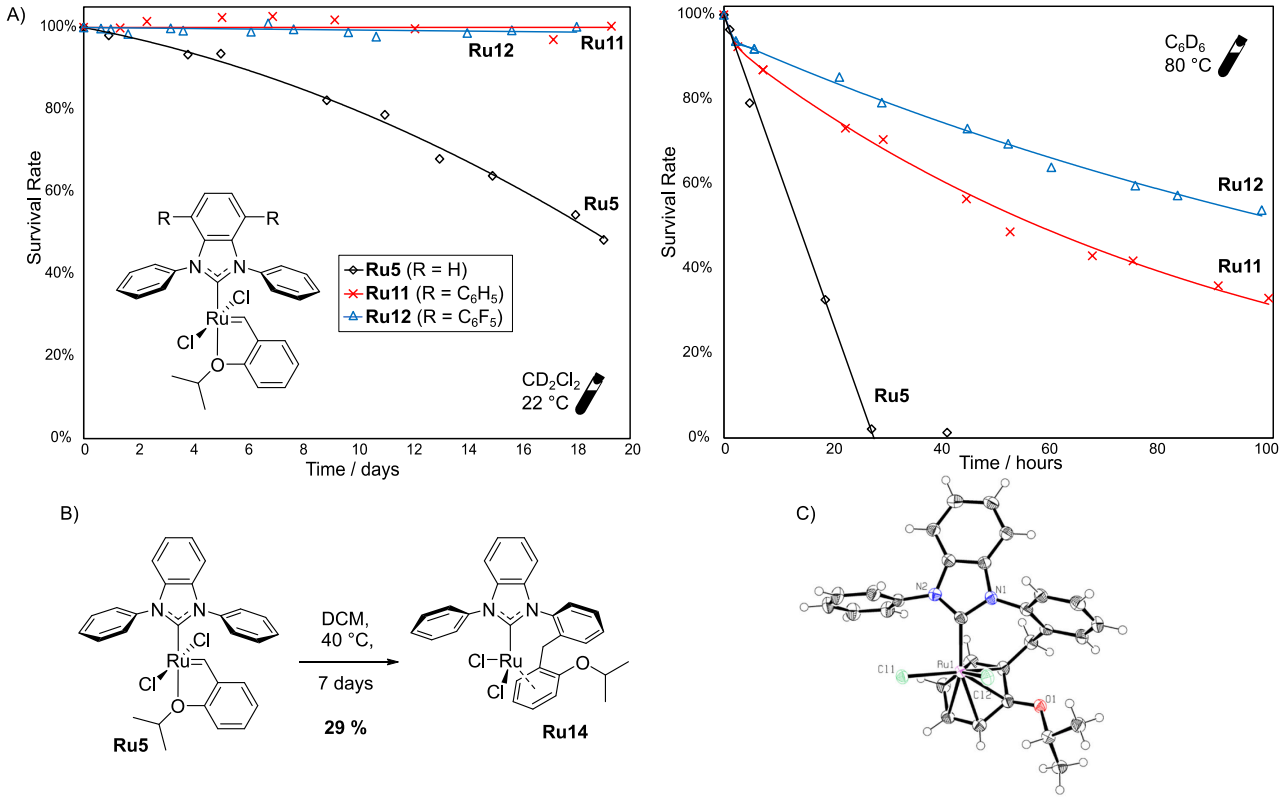

Figure 4. A) Stability test in solution at ambient and elevated temperature measured by ^{1}H NMR (1,3,5-trimethoxybenzene added as reference). Lines are visual aid only. Conditions: (left) CD_2Cl_2 at 22 °C, under argon; (right) C_6D_6 at 80 °C, under argon. B) Study of the decomposition of the complex **Ru5** into the complex **Ru14**. C) XRD structure of complex **Ru14** (ellipsoids are drawn at 50% probability).

Computational study. In order to explain the slower decomposition kinetics of complexes **Ru11** and **Ru12** compared to that of **Ru5**, we hypothesized that the insertion of an aromatic plane parallel to the *N*-aryl rings could prevent the rotation of the *N*-phenyl group in consequence constraining its aromatic CH activation and therefore its decomposition. Therefore, starting from complexes **5opt**, **11opt** and **12opt** we computed the TS Gibbs free energy barriers associated with the *N*-phenyl rotation (Figure 5), by DFT calculations at the B3PW91-D3 level of theory. Complexes **11opt and 12opt** display higher *N*-phenyl rotation TS energies (19.3 and 22.7 kcal·mol^{-1}) than compound **5opt** (17.4 kcal·mol^{-1}). This may be ascribed to the increased steric hindrance of compounds **11opt** and **12opt** compared to that of their simpler analog **5opt**. In addition, in agreement with the higher π-π stacking interaction expected between the *N*-phenyl and the second decker-pentafluorophenyl rings, the rotation of the *N*-phenyl ring is 3.4 kcal·mol^{-1} higher for **12opt** than for **11opt**. Thus, this TS energy trend well reflects the influence of both *i)* the increased steric bulk of **11opt** and **12opt** compared to **5opt** and *ii)* the F substitution on the strength of the phenyl-pentafluorophenyl π-π stacking interaction. However, the different catalyst deactivation kinetics measured for **5opt**, **11opt** and **12opt** cannot be ascribed to this *N*-phenyl rotation process, as the corresponding TS Gibbs free energy barriers can be easily overcome at room temperature, unlike experimentally observed.

Therefore, we wondered whether the slower decomposition of **Ru11** and **Ru12** at ambient temperature and the need for higher temperatures to observe their degradation could be instead ascribed to a particular step in the decomposition mechanism.

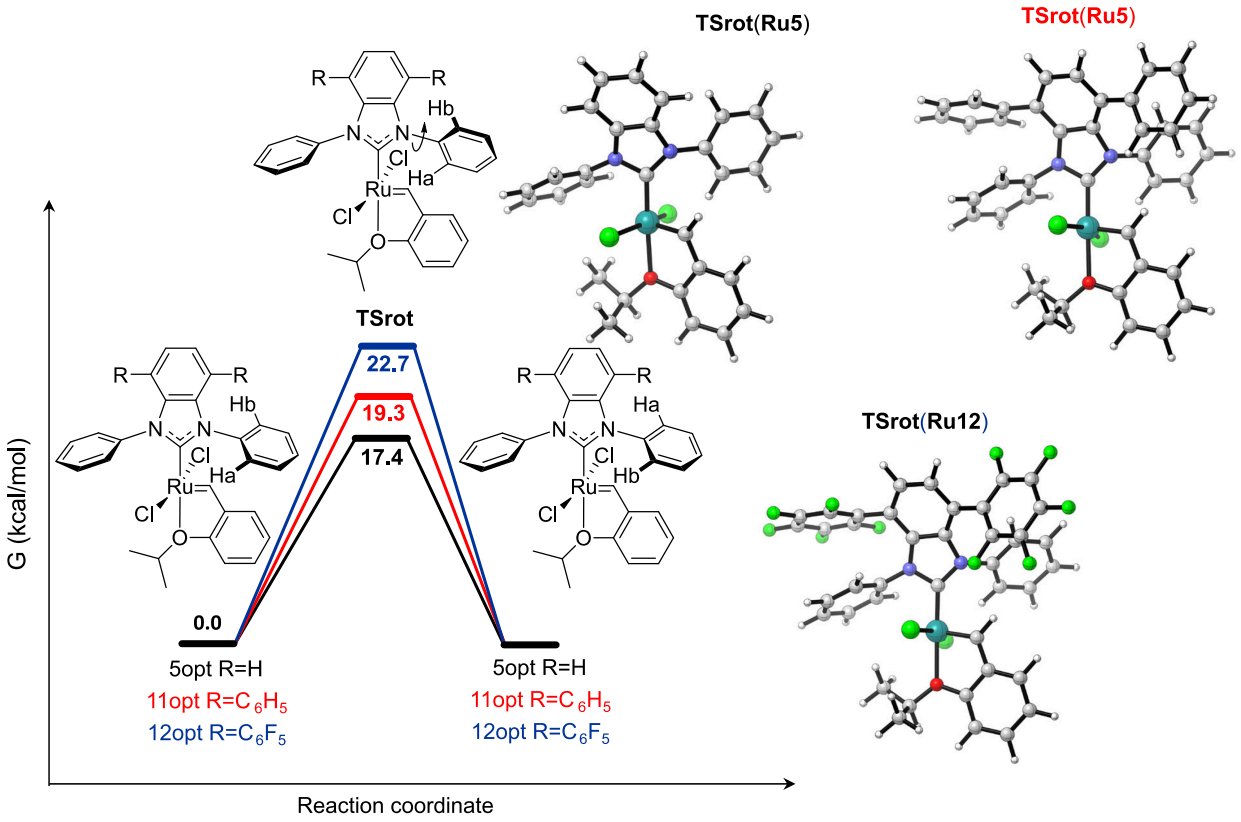

Figure 5. Calculated Gibbs free energy barrier associated with the rotation of *N*-phenyl substituent in complexes **5opt**, **11opt** and **12opt**, computed at the B3PW91-D3 level of theory.

Inspired by the work reported some years ago by the group of Cavallo for complex **Ru7** (Figure 1),[25,30] we thus performed the calculation of the whole decomposition pathway for compounds **Ru5**, **Ru11** and **Ru12**. For the sake of clarity in the comparison, their corresponding Gibbs free energy profiles are overlapped in Figures 6 and 7. Starting from compounds **5opt**, **11opt** and **12opt**, the first step involves a Berry pseudo rotation of the alkylidene O^{i}Pr arm bringing the O^{i}Pr group in *trans* position to one of the chloride ligands. The reaction is endergonic by 6.1, 10.1 and 8.8 kcal·mol^{-1}, with an associated barrier of 28.8, 33.8 and 33.4 kcal·mol^{-1}, for **TS-1**(**Ru5**), **TS-1**(**Ru11**) and **TS-1**(**Ru12**) respectively. Through a second Berry pseudo rotation process, one of the *N*-phenyl rings may then move in *trans* position to the alkylidene O^{i}Pr arm, engaging one of its *ortho*-C–H bonds into an agostic interaction with the Ru metal center. The reaction is endergonic by 24.2 and 28.1 kcal·mol^{-1} for **I-2**(**Ru5**) and both **I-2**(**Ru11**) and **I-2**(**Ru12**), respectively, the corresponding barriers measuring 27.6, 29.3 and 30.3 kcal·mol^{-1} for **TS-1**(**Ru5**), **TS-1**(**Ru11**) and **TS-1**(**Ru12**), respectively.

To prepare the H transfer from the *N*-phenyl cycle to the benzylidene group, the *N*-phenyl ring

must undergo a rotation, allowing the re-formation of an *ortho* C-H agostic interaction with the metal on the same side as the Ru-alkylidene bond. This rotation process is an equilibrium reaction, with the **I-3** intermediate lying at +1.0, −0.5 and −0.1 kcal·mol^{-1} relative to the **I-2** intermediate, for complexes **Ru5**, **Ru11** and **Ru12** respectively. In the next step, the transfer of the agostic activated proton to the nearby α-C atom of the benzylidene group may then occur, affording a Ru-benzyl complex containing a new σ-bond between the Ru center and the *ortho*-C atom of the NHC *N*-phenyl ring. Interestingly, while the barrier for the formation of the Ru···C-H agostic interaction through **TS-3** is almost identical between compound **Ru5** and compounds **Ru11** and **Ru12** (31.4, 33.7 and 32.6 kcal·mol^{-1}, respectively), the barrier for the transfer of the agostic activated proton to the benzylidene group through **TS-4** is considerably higher for complexes **Ru11** and **Ru12** (35.1 and 36.1 kcal·mol^{-1}) than for **Ru5** (28.1 kcal·mol^{-1}). This difference of 7.0 and 8.0 kcal·mol^{-1} between the **TS-4** energy of **Ru11** and **Ru12** with that of **Ru5** is probably due to the presence of the two parallelly stacked aryl rings on the benzimidazolylidene backbone which rigidify the NHC skeleton, thus reducing the flexibility of the *N*-phenyl ring during the proton transfer process in **TS-4**. In the corresponding products, lying at 21.3, 28.5 and 29.2 kcal·mol^{-1} for complexes **Ru5**, **Ru11**, and **Ru12** respectively, the benzylidene group is transformed into a benzyl group and a new Ru-C bond with an ortho position of the *N*-phenyl ring is created.

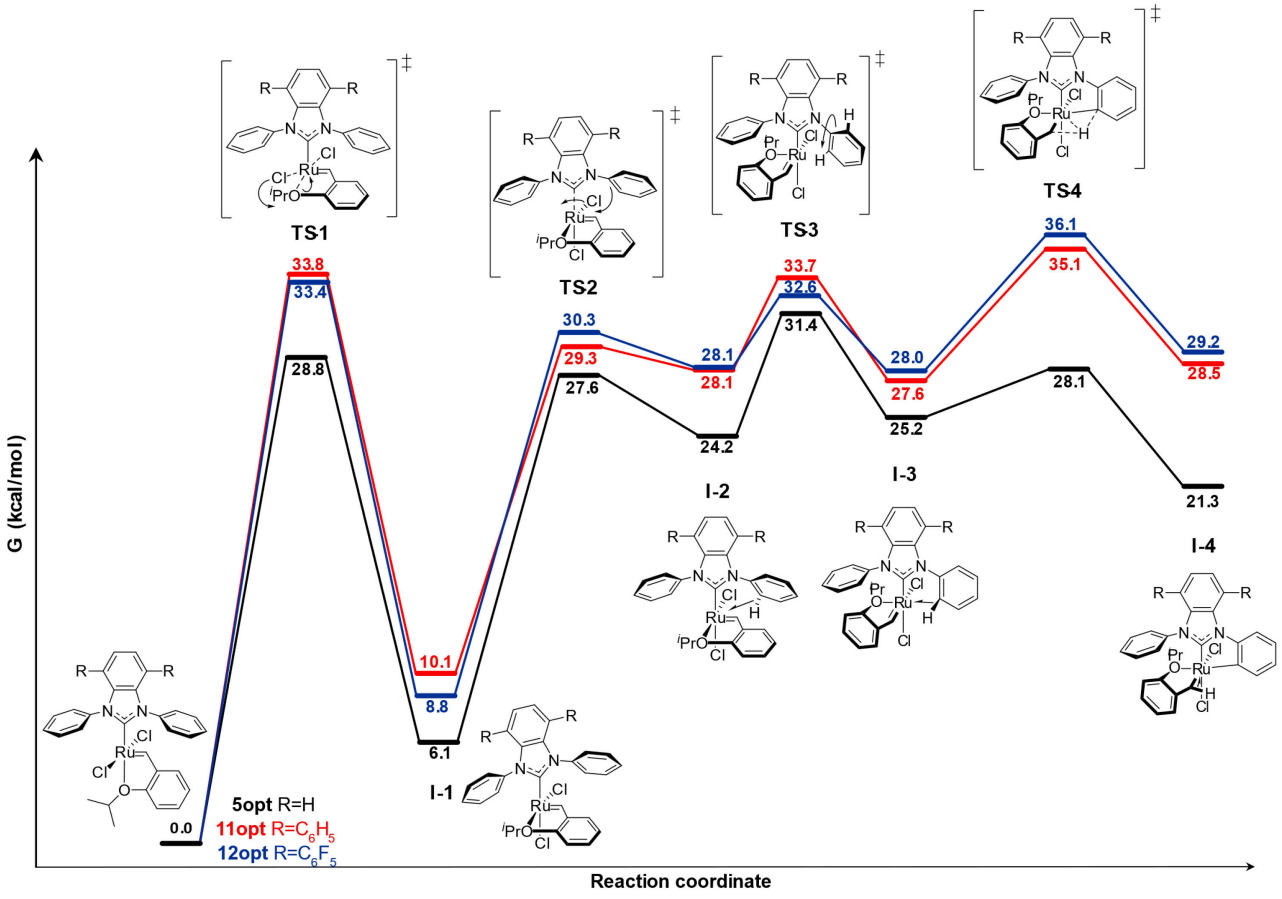

Figure 6. The first part of the Gibbs Free energy profile for the deactivation reaction of catalysts **Ru5** (black), **Ru11** (red) and **Ru12** (blue), computed at the B3PW91-D3 level of theory.

From intermediate **I-4**, a Berry pseudo rotation brings the benzyl O^{i}Pr arm in *trans* position to the NHC ring, affording intermediate **I-4'** by an equilibrium process (Figure 7). The following step involves, in a single step, both *i)* the transfer of an α hydrogen from the benzyl group to the Ru atom and *ii)* the insertion of the newly formed benzylidene into the σ-bond of the Ru-C_{ortho} atom of the *N*-phenyl ring. For complexes **Ru5**, **Ru11**, and **Ru12** respectively, this elementary step is exergonic by 6.9, 10.4 and 13.8 kcal·mol^{-1}, with the corresponding transition state measuring 29.7, 34.7 and 33.7 kcal·mol^{-1}.

The resulting intermediate **I-5** may then undergo a reductive elimination step which breaks the Ru–hydride bond, by transferring the hydrogen to the formerly benzylic C center. This leads to intermediate **I-6** with associated barriers of 20.2, 22.4 and 24.4 kcal·mol^{-1} for complexes **Ru5**, **Ru11** and **Ru12** respectively. Intermediate **I-6** is only a kinetic intermediate to the decomposition product **I-8**, which can be reached from **I-6** through a series of haptotropic shifts involving the Ru atom and the Ph group of the formerly benzylidene moiety, as confirmed by the X-Ray structure of complex **Ru14** (Figure 4). The formation of **I-8** is slightly exergonic by only −3.2, −0.2, and −2.3 kcal·mol^{-1} for compounds **Ru5**, **Ru11**, and **Ru12**, respectively, in contrast to the stability of about 20 kcal·mol^{-1} obtained for the analog of complex **Ru5**, which contains the same benzylidene ligand without the O^{i}Pr substituent (**Ru10**, Figure 1).[25] This difference is likely to be ascribed to the decoordination of the O^{i}Pr ligand during the formation of the final η^6 product **I-8**, which destabilizes the system with respect to the starting compound.

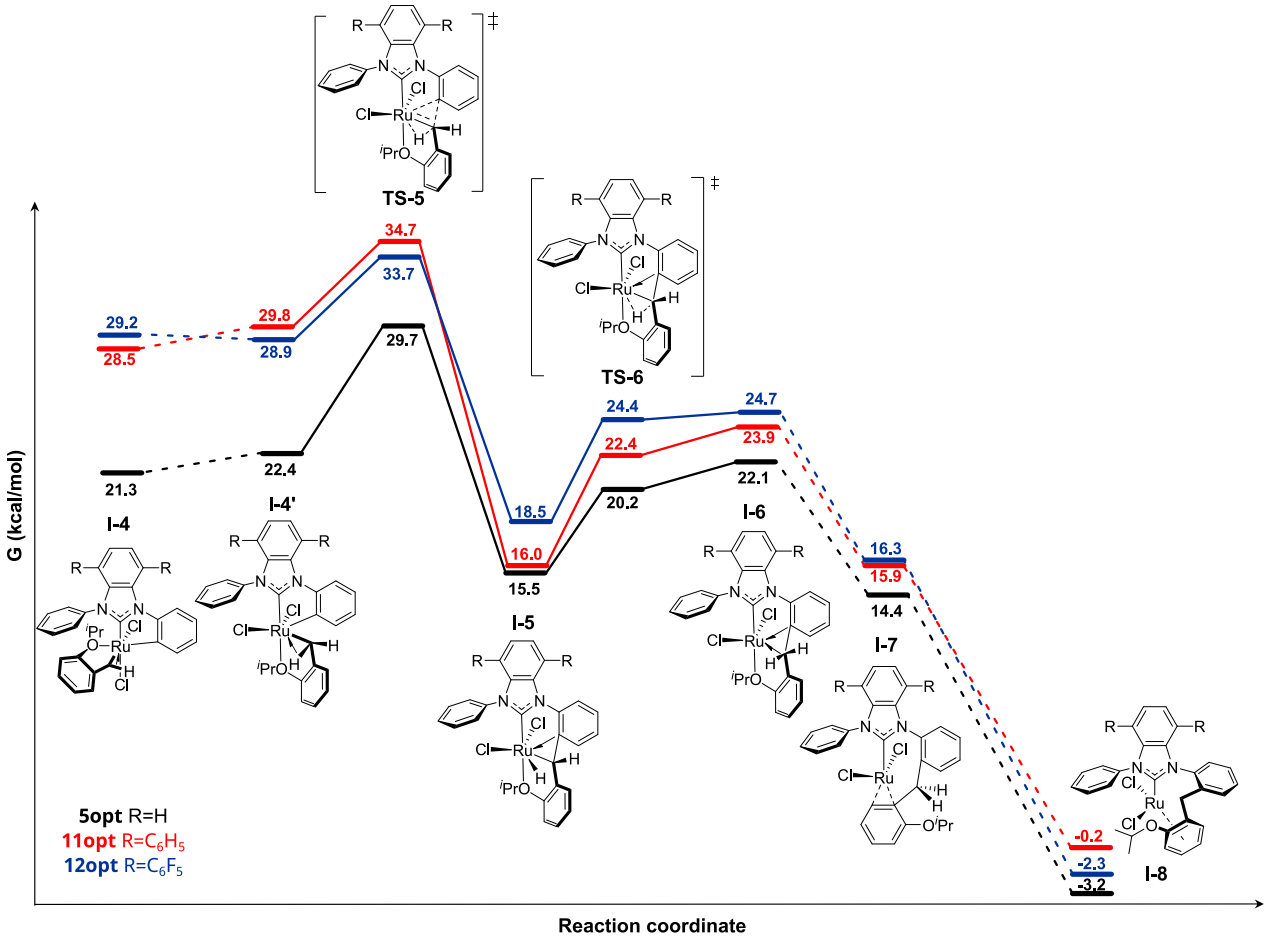

Figure 7. The second part of the Gibbs Free energy profile for the deactivation reaction of catalysts **Ru5** (black), **Ru11** (red), and **Ru12** (blue), computed at the B3PW91-D3 level of theory.

Considering the full mechanistic profile, the path between intermediates **I-3** and **I-5** involves transition states with the Gibbs free energy values of **Ru11** and **Ru12** considerably higher than those of **Ru5**. This indicates that the influence of the insertion of an aromatic plane parallel to the *N*-phenyl rings seems to have a particularly significant impact on the **TS-4** and **TS-5** transition states. Therefore, we carried out a geometrical analysis of structures of those key transition states for compounds **Ru5**, **Ru11** and **Ru12** displaying in Figure 8 the most significant geometrical parameters.

In all the three TS-4 transition states (Figure 8A), the aromatic *N*-phenyl ring is heavily rotated, so that the activated C–H bond can properly interact with the Ru center and thus be transferred to the alkylidene moiety, the C9-H and C49-H bond distances measuring 2.023, 2.092, 2.056 Å and 1.645, 1.599, 1.616 Å for complexes **Ru5**, **Ru11** and **Ru12** respectively. As a consequence, the *N*-phenyl ring arranges in a quasi-coplanar fashion with respect to the benzimidazolylidene heterocycle, and any substitution on the benzimidazolylidene moiety results in a steric clash that disfavors the *N*-phenyl rotation, increasing the **TS-4** energy. This increased steric repulsion is geometrically traduced by an out-of-plane distortion of the two benzimidazolylidene rings. Indeed, while in **TS-**

4(**Ru5**) the two rings of the bicyclic benzimidazolylidene are almost perfectly planar (dihedral angles N2-C7-C2-N1 = 0.5°, C6-C7-C2-C3 = 0.9°), they clearly deviate from planarity in **TS-4**(**Ru11**) and **TS-4**(**Ru12**) (N2-C7-C2-N1 = 5.7° and 5.5°, C6-C7-C2-C3 = 9.5° and 10.3° respectively), due to the steric clash between the *N*-phenyl and C-aryl groups upon rotation around the N-C_{Ph} bond. The crossing of this transition state, therefore, requires more energy for complexes **Ru11** and **Ru12** than for **Ru5**, reflecting their slower experimental decomposition shown in Figure 4.

Figure 8B shows the geometry of the transition states **TS-5** of compounds **Ru5**, **Ru11** and **Ru12**. While for **TS-5**(**Ru5**) the C-C bond formation occurs once the benzylic H has been already transferred to the Ru center, in the case of **Ru11** and **Ru12** these two processes occur simultaneously. As previously seen for **TS-4**, the kinetic barrier associated with **TS-5** is considerably higher for complexes **Ru11** and **Ru12** (34.7 and 33.7 kcal·mol^{-1}) than for **Ru5** (29.7 kcal·mol^{-1}), and arises from the same distortion of the benzimidazolylidene core due to steric clash between the stacked exocyclic aryl groups.

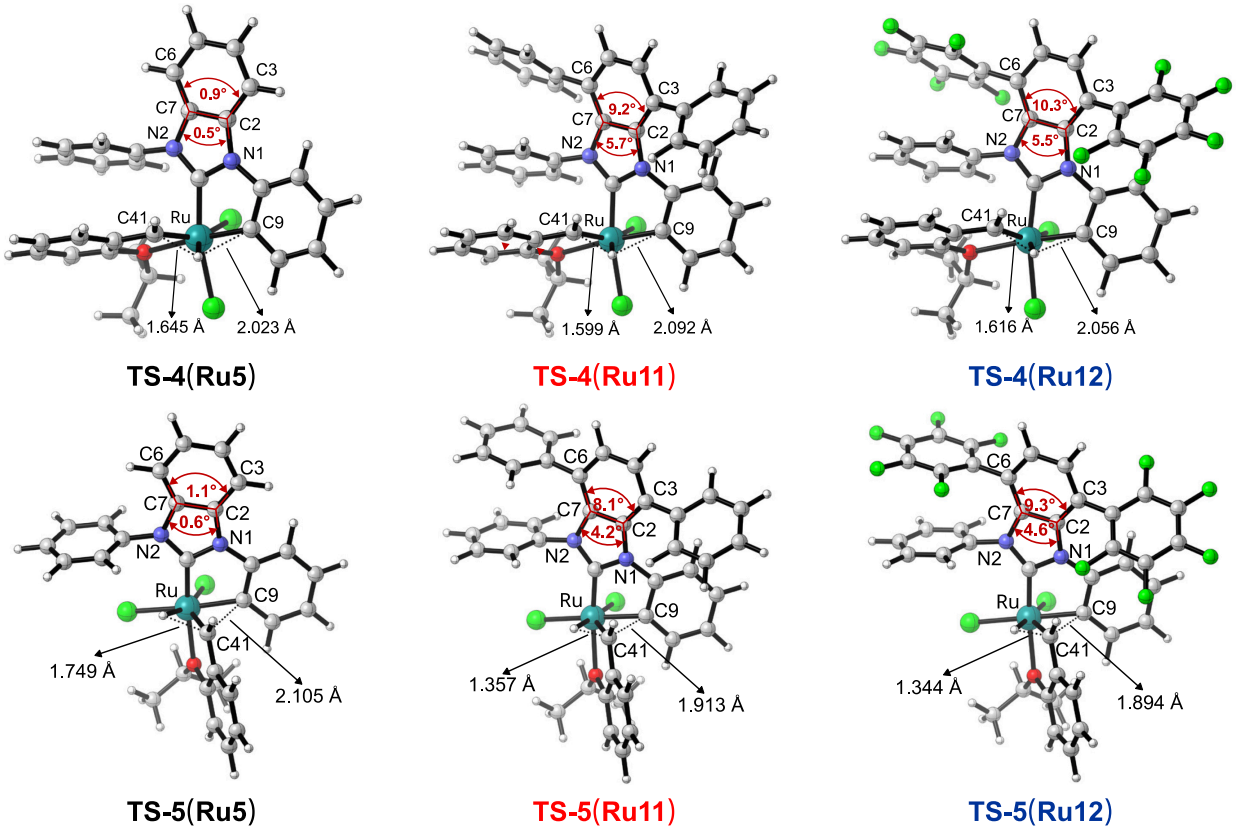

Figure 8. Geometrical parameters of the **TS-4** and **TS-5** structure of complexes **Ru5**, **Ru11** and **Ru12**.

In conclusion, therefore, the computed decomposition profile indicates that the steric repulsion between the *N*-phenyl and the second decker phenyl- and pentafluorophenyl groups strongly affects the rate-determining step of the reaction which involves *i)* the transfer of the *N*-phenyl agostic proton to the nearby α-C atom of the benzylidene group (**TS-4**) and *ii)* the transfer of the benzylic

H to Ru coupled with the C-C bond formation (**TS-5**). The corresponding kinetic barrier is thus considerably higher for compounds **Ru11** and **Ru12** than for **Ru5**, in accordance with the decomposition kinetics reported in Figure 4.

Catalytic activity studies. The catalytic performance of the new, "stacked" complexes was compared with known benchmark **Ru5** using a set of model reactions. First, we checked their activity in ring closing metathesis (RCM) with tetrasubstituted C-C double bond formation. [13,14] For this purpose, diethyl 2,2-di(2-methylallyl)malonate (**10a**) was chosen as the model substrate and the time-conversion plots of its RCM reaction were constructed with 0.2 mol% of each catalyst, in toluene, at 80 °C (Figure 9). All complexes exhibited high activity, affording considerable conversions within the first 30 minutes. **Ru5** is one of the most active catalysts designed for this reaction,[17] and the new catalysts bear the same small *N*-substituents at the NHC ligands. Thus said, the reaction catalyzed by **Ru5** reached its limits at a significantly lower conversion than that recorded with **Ru11** and **Ru12**. This can be attributed to a more stable 14-e$^-$ catalytic species formed from the latter catalysts versus those generated from **Ru5**. Interestingly, although **Ru11** gave higher conversions than **Ru12** within the first hour of the reaction, after this point the trend reversed, leading to 96% conversion with **Ru12** versus 91% with **Ru11** after 5 hours (and 72% for the benchmark **Ru5**).

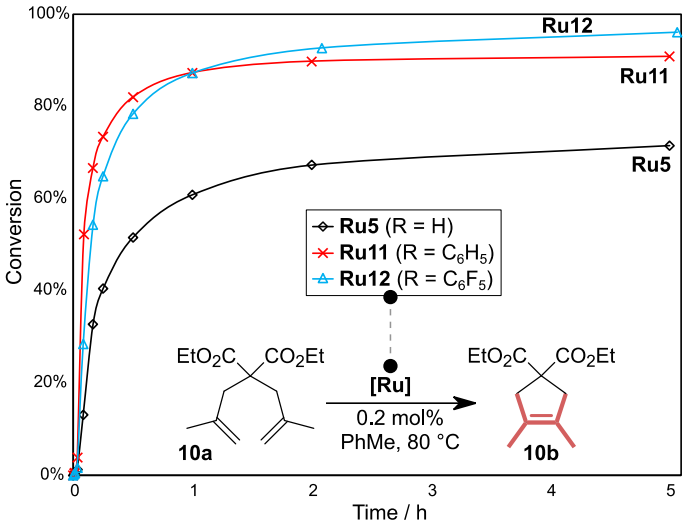

Figure 9. Time-conversion curves in RCM of diene **10a**. Conditions: catalyst 0.2 mol%, PhMe, 80 °C under argon. Measured by GC with 1,3,5-trimethoxybenzene added as internal standard. Lines are visual aid only.

To further examine the differences in catalyst productivity, the previously described reaction of **10a** was reattempted at *two times lower catalyst loading* of 0.1 mol% (Scheme 4). The trend observed earlier was maintained and **Ru5** gave a rather poor conversion for such reaction (50%), whereas **Ru11** and **Ru12** gave much higher conversions of 81% and 92%, respectively. The three **BIPh**-type

catalysts were further tested in five more challenging RCM reactions featuring tetrasubstituted double C-C bond formation. Similar was the case of the formation of the six-membered malonate **11b** and five-membered tosylamide **13b** where **Ru11** and **Ru12** gave up to 32 percentage points (%p) higher substrate conversions compared to **Ru5**. The fluorinated complex **Ru12** slightly but noticeably outperformed **Ru11** in the two latter reactions. The superiority of the new catalysts **Ru11** and **Ru12** was even more pronounced in the more challenging formation of a less thermodynamically favored seven-membered ring (compounds **12b** and **14b**). In these latter cases, a much higher catalyst loading of 2 mol% with malonate **12a** and 1 mol% with tosylamide **14a** was required to reach suitable conversions[56,13,14] and it is worth noting that **Ru11** and **Ru12** gave conversions 4-8 times higher than **Ru5**. Again, **Ru12** was slightly better than **Ru11** which overall correlates with the observed trend in stability tests.

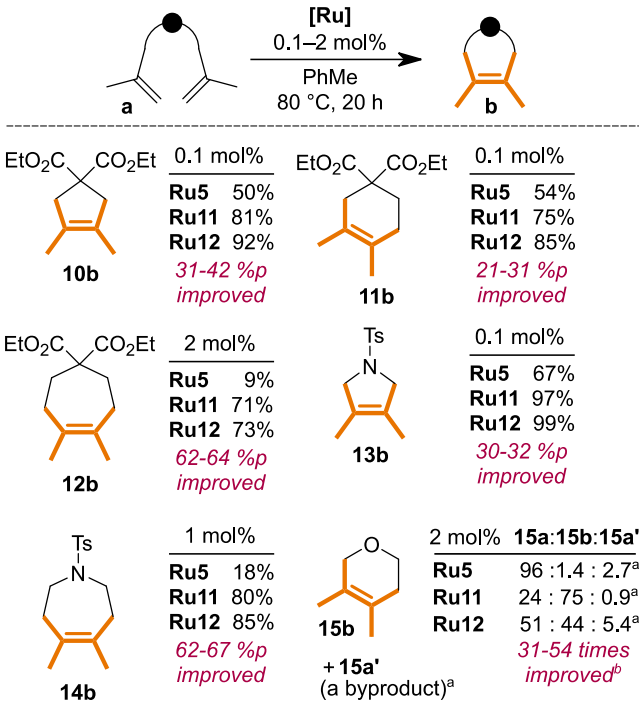

Scheme 4. Scope and limitations of catalysts **Ru5**, **Ru11**, and **Ru12** in RCM of challenging substrates. %p – percentage point difference from **Ru5** in a substrate conversion, determined by gas chromatography; [a] by-product **15a**' was formed (see Figure 10), reaction was conducted for 8 h; [b] improvement in formation of main product **15b** from replacing **Ru5** with **Ru11** or **Ru12** .

For all substrates discussed so far, the desired RCM products were obtained as the sole product. However, the RCM reaction of ether **15a** led to the formation of a rearranged byproduct **15a'** resulting from a double bond migration along the alkyl chain (Scheme 4 and Figure 10A). This can be caused by catalyst decomposition products (probably ruthenium hydride species).[57-59] The observed formation of **15a'** stands in agreement with the previous report of Grubbs and co-workers, although

this isomerization product was not characterized there.[17] Catalyst **Ru5** offered a very poor conversion of **15a**, forming **15b** and **15a'** in comparable amounts (**15a**:**15b**:**15a'**ratio of 96:1.4:2.7). Interestingly, in this example **Ru11** outperformed **Ru12**, both in terms of conversion and selectivity toward **15b** (**15a**:**15b**:**15a'** ratio for **Ru11** reached 24:75:0.9 versus 51:44:5.4 for **Ru12** after 8 hours at 80 °C). This observation could be explained by the subtle difference in activity of **Ru11** and **Ru12** that was observed in RCM of **10a** (Figure 9).

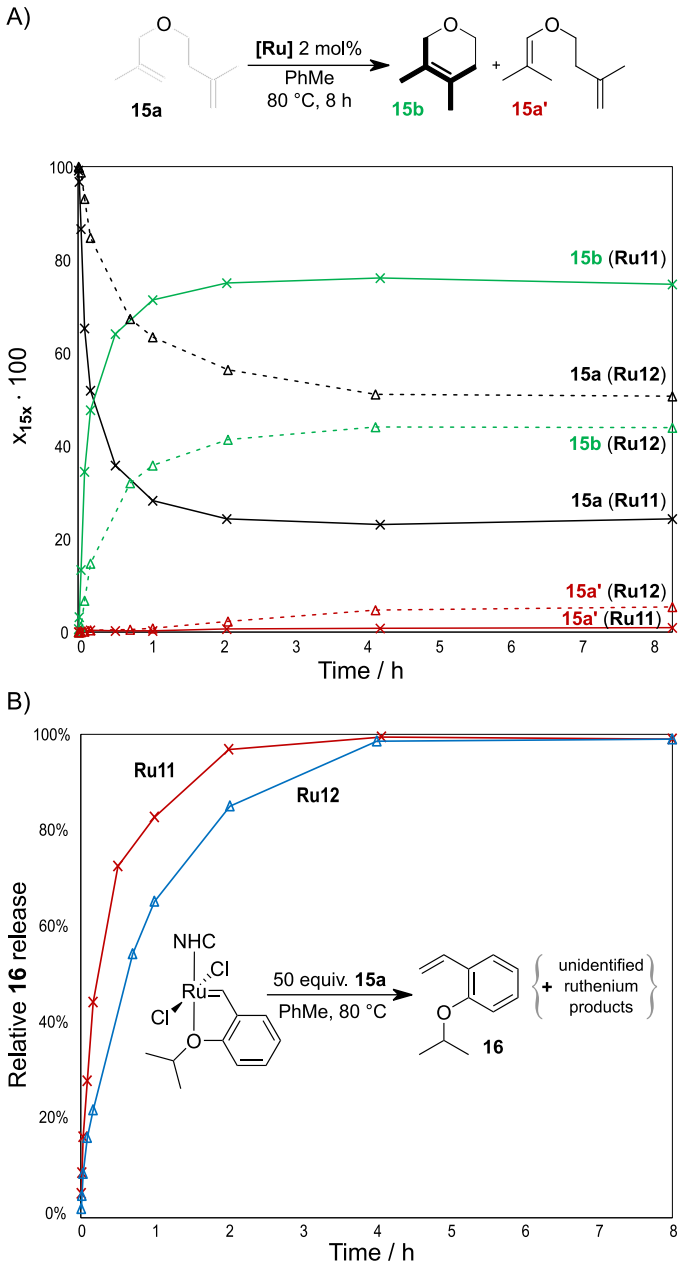

Figure 10. A) Reaction profile of substrate **15a** RCM. B) *o*-isopropoxystyrene (**16**) release during RCM of diene **15a**.

To verify the latter hypothesis, the reaction profile for RCM of **15a** was established, comparing **Ru11** performance with **Ru12** (Figure 10A). The difference in catalyst activity is more pronounced in this challenging RCM example, and complex **Ru11** is considerably more active than **Ru12**

(**15a**:**15b**:**15a'** ratio after 1 h reached 28:71:0.3 with **Ru11** versus 63:36:0.8 with **Ru12**). After the first hour of the reaction, the formation of **15b** slows significantly, indicating that most of the catalytically active species has been spent. After that point, the formed decomposition products start to isomerize **15a,** which is available in a higher quantity in the case of the reaction with **Ru12**. Those factors account for a higher amount of **15a'** observed with **Ru12** after 8 h.

To further probe the origin of **Ru11** higher activity, the release of *o*-isopropoxystyrene (**16**) (relative to the last point measured at 8 h) versus time was plotted (Figure 10B). The formation of **16** can serve as an indirect measure of how catalyst initiation progresses throughout the reaction. For both complexes, **16** release finishes within the first 4 h, although for **Ru11** the slope is considerably steeper than for **Ru12**. This is in line with the hypothesis that **Ru11** is a more active catalyst than **Ru12** probably due to a faster initiation rate resulting from a higher *trans* effect of more electron donating **BI*Ph** NHC ligand.

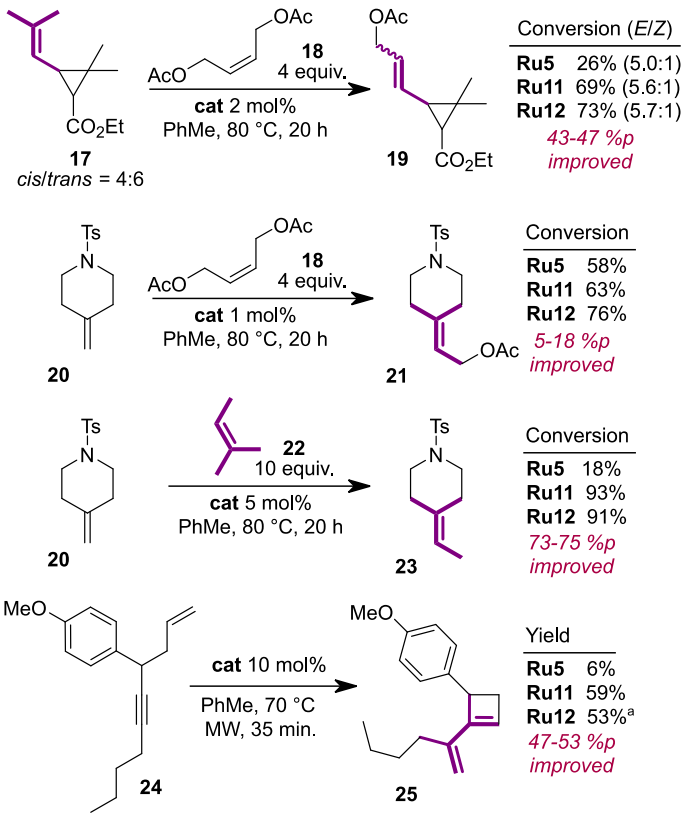

Scheme 5. Scope and limitations of catalysts **Ru5**, **Ru11**, and **Ru12** in CM and cycloisomerization of challenging substrates. [a] Reaction conducted in perfluorotoluene. %p – percentage point difference from **Ru5**.

To further evaluate the scope and limitations of catalysts **Ru11** and **Ru12**, several challenging cross metathesis (CM) reactions were investigated (Scheme 5). First, we studied the reaction between ethyl chrysanthemate (**17**) and *Z*-1,4-diacetoxy-2-butene (**18**). The challenge of this transformation lies in the low reactivity of the trisubstituted double C-C bond in **17**.[27] Catalysts **Ru11** and **Ru12** gave similar conversions of **17**, 69% and 73% respectively, giving product **19** selectively, whereas

known **Ru5** provided only 26% of conversion. Next, the functionalization of the geminal C-C double bond of 4-methylene-1-tosylpiperidine (**20**) with either **18** or amylene (**22**) was probed. In the case of reaction with **18**, the use of **Ru11** and **Ru12** allowed for conversions up to 18 percent-points (%p) higher compared to benchmark **Ru5**, leading to 76% conversion for **Ru12**.

Noteworthy, in the example of CM of **20** with amylene,[60,61] the double-decker NHC catalysts **Ru11** and **Ru12** gave almost quantitative conversions of **20**, 93% and 91% respectively, which was 5 times higher than in the case of **Ru5** reaching only 18%. Last but not least, the highly challenging 1,5-enyne metathesis of substrate **24** to obtain crowded and strained cyclobutene derivative **25** was attempted.[62] An additional difficulty arising in this reaction is that its selectivity can be compromised by a competing self-CM side reaction and by degradation of the highly strained resulting product. We were pleased to find that catalysts **Ru11** and **Ru12** gave good yields of 59% and 53% respectively, whereas with **Ru5** only traces of product were observed which amounted to 6% yield. Interestingly, similarly to the case of the RCM reaction of **15a**, in this example, catalyst **Ru11** performed visibly better than its fluorinated counterpart **Ru12**, which we attribute to **Ru11** higher activity. Remarkably, the use of the new catalysts allowed for a two-fold diminution in catalyst loading compared to the general-purpose **SIMes** complex **Ru2** used at 20 mol% loading.[62]

CONCLUSION

In summary, we developed the two new biplane-type NHC ligands **BI*Ph** and **BIF*Ph** based on a benzimidazolylidene core, whose lower wings are set as *N*-phenyl rings to reduce their steric hindrance on the first coordination sphere and whose upper wings are phenyl or pentafluorophenyl rings, respectively. The corresponding second-generation Grubbs-Hoveyda complexes **Ru11** and **Ru12** were generated and the effect of the introduction of the second decker of aromatic rings on their stereoelectronic properties, stability, and catalytic efficiency was evaluated, taking the monoplane-type, unsubstituted **BIPh** ligand as a reference. According to the nature of the aromatic rings, **BI*Ph** was shown to be more electron-donating than **BIPh**, while **BIF*Ph** is less donating. Conversely, the second aromatic decker led in both cases to slightly less hindered NHC ligands compared to **BIPh** by forcing the *N*-phenyl rings to stay in a more orthogonal position relative to the benzimidazolylidene core.

More importantly, both complexes **Ru11** and **Ru12** *were shown to be significantly more stable* than the known **BIPh**-supported complex **Ru5**. This stability gain was rationalized through DFT calculations of the decomposition pathways. Although the aromatic rings of the second decker cannot stop the rotation of the *N*-phenyl groups in **Ru11** and **Ru12**, they strongly contribute to the increase in energy of the rate-determining step, by forcing a strong distortion of the carbenic heterocycle through steric constraints. The rate-determining step involves proton transfer of one of the

ortho positions of the *N*-phenyl groups to the nearby carbon atom of the benzylidene moiety followed by migration of the benzylic proton to ruthenium with the simultaneous carbon-carbon bond formation. Moreover, the observed increased stability of the ruthenium precursors **Ru11** and **Ru12** was also translated to the active species and enabled their implementation as highly efficient, stable pre-catalysts in challenging olefin metathesis reactions for the formation of tri- and tetra-substituted C-C double bonds. Complex **Ru11** bearing the more electron-donating and *trans* effect inducting **BI*Ph** ligand revealed also more active than its **Ru12** counterpart bearing the less electron donating **BIF*Ph** ligand.

Overall, while it is well known that ruthenium catalysts bearing NHC ligands with low steric demand are more fragile, which impairs their productivity, we showed here that the adjunction of a second decker of aromatic groups in the NHC scaffold is a viable and promising strategy to access very stable and efficient olefin metathesis catalysts. Because the formation of sterically hindered olefins has always been the Achilles' heel of the ruthenium-catalyzed metathesis, this special trait exhibited by the newly obtained complexes appears of paramount importance. We believe that the present report will open up new possibilities for further developments of olefin metathesis catalysts and will significantly extend applications of this transformation in natural product synthesis and medicinal chemistry.

ACKNOWLEDGEMENTS

This work has received funding from the European Union's Horizon 2020 research and innovation programme under the Marie Skłodowska-Curie grant agreement No. 860322.

C. D. and I. d. R. are indebted to CALMIP for HPC resources (Grant 2017-[p17010]).

We are grateful to Ekaterina Gulyaeva for the creation of the graphical abstract.

CONFLICT OF INTEREST

The authors declare no conflict of interest.

SUPPORTING INFORMATION

Detailed experimental procedures, copies of NMR spectra, computational methods, Cartesian coor-

dinates of DFT-optimized structures, and crystallographic details. Crystal structures have been deposited with the Cambridge Crystallographic Data Centre CCDC). The data can be obtained free of charge via www.ccdc.cam.ac.uk/structures.

REFERENCES

1 Grela, K. in *Olefin Metathesis: Theory and Practice* (ed Karol Grela) (John Wiley & Sons, Inc., Hoboken, 2014).

2 Grubbs, R. H., Wenzel, Anna G., O'Leary, Daniel J., Khosravi, Ezat in *Handbook of Metathesis* (ed Robert H. Grubbs, Wenzel, Anna G., O'Leary, Daniel J., Khosravi, Ezat) (Wiley-VCH, 2015).

3 Hoveyda, A. H. & Zhugralin, A. R. The remarkable metal-catalysed olefin metathesis reaction. *Nature,* **2007**, *450*, 243-251.

4 Ogba, O. M., Warner, N. C., O'Leary, D. J. & Grubbs, R. H. Recent advances in ruthenium-based olefin metathesis. *Chem. Soc. Rev.,* **2018**, *47*, 4510-4544.

5 Nolan, S. P. & Cazin, C. S. J. *N-Heterocyclic Carbenes in Catalytic Organic Synthesis* (Thieme Chemistr, 2017).

6 Hopkinson, M. N., Richter, C., Schedler, M. & Glorius, F. An overview of N-heterocyclic carbenes. *Nature,* **2014**, *510*, 485-496.

7 Smith, C. A. *et al.* N-Heterocyclic Carbenes in Materials Chemistry. *Chem. Rev.,* **2019**, *119*, 4986-5056.

8 Zhao, Q., Meng, G., Nolan, S. P. & Szostak, M. N-Heterocyclic Carbene Complexes in C–H Activation Reactions. *Chem. Rev.,* **2020**, *120*, 1981-2048.

9 Peris, E. Smart N-Heterocyclic Carbene Ligands in Catalysis. *Chem. Rev.* **2018**, *118*, 9988-10031.

10 Huynh, H. V. Electronic Properties of N-Heterocyclic Carbenes and Their Experimental Determination. *Chem. Rev.* **2018**, *118*, 9457-9492.

11 Samojłowicz, C., Bieniek, M. & Grela, K. Ruthenium-Based Olefin Metathesis Catalysts Bearing N-Heterocyclic Carbene Ligands. *Chem. Rev.* **2009**, *109*, 3708-3742.

12 Vougioukalakis, G. C. & Grubbs, R. H. Ruthenium-Based Heterocyclic Carbene-Coordinated Olefin Metathesis Catalysts. *Chem. Rev.* **2009**, *110*, 1746-1787.

13 Mukherjee, N., Planer, S. & Grela, K. Formation of tetrasubstituted C–C double bonds via olefin metathesis: challenges, catalysts, and applications in natural product synthesis. *Org. Chem. Front.* **2018**, *5*, 494-516.

14 Lecourt, C. *et al.* Natural products and ring-closing metathesis: synthesis of sterically congested olefins. *Nat. Prod. Rep.* **2018**, *35*, 105-124.

15 This limitation is particularly unfavorable in the context of total synthesis of natural and biologically active compounds, see: Wang, Y., Nagai, T., Watanabe, I., Hagiwara, K. & Inoue, M. Total Synthesis of Euonymine and Euonyminol Octaacetate. *J. Am. Chem. Soc.* **2021**, *143*, 21037-21047.

16 Stewart, I. C. *et al.* Highly Efficient Ruthenium Catalysts for the Formation of Tetrasubstituted Olefins via Ring-Closing Metathesis. *Org. Lett.* **2007**, *9*, 1589-1592.

17 Berlin, J. M. *et al.* Ruthenium-Catalyzed Ring-Closing Metathesis to Form Tetrasubstituted Olefins. *Org. Lett.* **2007**, *9*, 1339-1342.

18 Ragone, F., Poater, A. & Cavallo, L. Flexibility of N-Heterocyclic Carbene Ligands in Ruthenium Complexes Relevant to Olefin Metathesis and Their Impact in the First Coordination Sphere of the Metal. *J. Am. Chem. Soc.* **2010**, *132*, 4249-4258.

19 Vehlow, K., Gessler, S. & Blechert, S. Deactivation of Ruthenium Olefin Metathesis Catalysts through Intramolecular Carbene–Arene Bond Formation. *Angew. Chem. Int. Ed.* **2007**, *46*, 8082-8085.

20 A conceptually different idea for forcing tetrasubstituted C=C bonds formation in olefin metathesis is to use specially reinforced SIMes-bearing catalysts at higher temperatures (up to 140 °C), eg. Refs. 21-22.
21 Bantreil, X., Schmid, T. E., Randall, R. A. M., Slawin, A. M. Z. & Cazin, C. S. J. Mixed N-heterocyclic carbene/phosphite ruthenium complexes: towards a new generation of olefin metathesis catalysts. *Chem. Commun.* **2010**, *46*, 7115-7117.
22 Vorfalt, T., Leuthäußer, S. & Plenio, H. An [(NHC)(NHC_{EWG})$RuCl_2$(CHPh)] Complex for the Efficient Formation of Sterically Hindered Olefins by Ring-Closing Metathesis. *Angew. Chem. Int. Ed.* **2009**, *48*, 5191-5194.
23 Hong, S. H., Chlenov, A., Day, M. W. & Grubbs, R. H. Double C-H Activation of an N-Heterocyclic Carbene Ligand in a Ruthenium Olefin Metathesis Catalyst. *Angew. Chem. Int. Ed.* **2007**, *46*, 5148-5151.
24 Mathew, J., Koga, N. & Suresh, C. H. C–H Bond Activation through σ-Bond Metathesis and Agostic Interactions: Deactivation Pathway of a Grubbs Second-Generation Catalyst. *Organometallics,* **2008**, *27*, 4666-4670.
25 Poater, A. & Cavallo, L. Mechanistic insights into the double C–H (de)activation route of a Ru-based olefin metathesis catalyst. *J. Mol. Catal. A Chem.* **2010**, *324*, 75-79.
26 Torborg, C. *et al.* Stable ruthenium indenylidene complexes with a sterically reduced NHC ligand. *Chem. Commun.* **2013**, *49*, 3188-3190.
27 Planer, S., Małecki, P., Trzaskowski, B., Kajetanowicz, A. & Grela, K. Sterically Tuned N-Heterocyclic Carbene Ligands for the Efficient Formation of Hindered Products in Ru-Catalyzed Olefin Metathesis. *ACS Catal.* **2020**, *10*, 11394-11404.
28 Ivry, E. *et al.* Light- and Thermal-Activated Olefin Metathesis of Hindered Substrates. *Organometallics*, **2018**, *37*, 176-181.
29 Kośnik, W. *et al.* Ruthenium Olefin Metathesis Catalysts Bearing a Macrocyclic N-Heterocyclic Carbene Ligand: Improved Stability and Activity. *Angew. Chem. Int. Ed.* **2022**, *61*, e202201472.
30 Poater, A., Bahri-Laleh, N. & Cavallo, L. Rationalizing current strategies to protect N-heterocyclic carbene-based ruthenium catalysts active in olefin metathesis from C–H (de)activation. *Chem. Commun.* **2011**, *47*, 6674-6676.
31 Chung, C. K. & Grubbs, R. H. Olefin Metathesis Catalyst: Stabilization Effect of Backbone Substitutions of N-Heterocyclic Carbene. *Org. Lett.* **2008**, *10*, 2693-2696.
32 Kuhn, K. M., Bourg, J.-B., Chung, C. K., Virgil, S. C. & Grubbs, R. H. Effects of NHC-Backbone Substitution on Efficiency in Ruthenium-Based Olefin Metathesis. *J. Am. Chem. Soc.* **2009**, *131*, 5313-5320.
33 Borguet, Y., Zaragoza, G., Demonceau, A. & Delaude, L. Ruthenium catalysts bearing a benzimidazolylidene ligand for the metathetical ring-closure of tetrasubstituted cycloolefins. *Dalton Trans.* **2015**, *44*, 9744-9755.
34 Borguet, Y., Zaragoza, G., Demonceau, A. & Delaude, L. Assessing the ligand properties of 1,3-dimesitylbenzimidazol-2-ylidene in ruthenium-catalyzed olefin metathesis. *Dalton Trans.* **2013**, *42*, 7287-7296.
35 Lv, T., Wang, Z., You, J., Lan, J. & Gao, G. Copper-Catalyzed Direct Aryl Quaternization of N-Substituted Imidazoles to Form Imidazolium Salts. *J. Org. Chem.* **78**, 5723-5730 (2013).
36 Kang, S.-K., Lee, S.-H. & Lee, D. Copper-Catalyzed N-Arylation of Amines with Hypervalent Iodonium Salts. *Synlett,* **2000**, *2000*, 1022-1024.
37 Examples of N-R substituted imidazole arylations to corresponding imidazolium salts can be found in the literature, e.g. ref. 35 as well as arylations from NH imidazoles to corresponding N-aryl imidazoles, ref. 36.
38 Verlinden, K., Buhl, H., Frank, W. & Ganter, C. Determining the Ligand Properties of N-Heterocyclic Carbenes from 77Se NMR Parameters. *Eur. J. Inorg. Chem.* **2015**, *2015*, 2416-2425.
39 Names for substituted BIPh NHC ligands were adopted in analogy with well-known Cp and Cp* naming scheme.

40 Wohlrab, A., Lamer, R. & VanNieuwenhze, M. S. Total Synthesis of Plusbacin A3: A Depsipeptide Antibiotic Active Against Vancomycin-Resistant Bacteria. *J. Am. Chem. Soc.* **2007**, *129*, 4175-4177.
41 Iglesias, M. *et al.* Synthesis and Structural Features of Rhodium Complexes of Expanded Ring N-Heterocyclic Carbenes. *Eur. J. Inorg. Chem.* **2009**, *2009*, 1913-1919.
42 Vummaleti, S. V. C. *et al.* What can NMR spectroscopy of selenoureas and phosphinidenes teach us about the π-accepting abilities of N-heterocyclic carbenes? *Chem. Sci.* **2015**, *6*, 1895-1904.
43 Garber, S. B., Kingsbury, J. S., Gray, B. L. & Hoveyda, A. H. Efficient and Recyclable Monomeric and Dendritic Ru-Based Metathesis Catalysts. *J. Am. Chem. Soc.* **2000**, *122*, 8168-8179.
44 Deposited at the Cambridge Crystallographic Data Centre (CCDC) under accession number 1100116.
45 Zhang, Y., Lavigne, G., Lugan, N. & César, V. Buttressing Effect as a Key Design Principle towards Highly Efficient Palladium/N-Heterocyclic Carbene Buchwald–Hartwig Amination Catalysts. *Chem. Eur. J.* **2017**, *23*, 13792-13801.
46 Deposited at the Cambridge Crystallographic Data Centre (CCDC) under accession number 605939.
47 Addison, A. W., Rao, T. N., Reedijk, J., van Rijn, J. & Verschoor, G. C. Synthesis, structure, and spectroscopic properties of copper(II) compounds containing nitrogen–sulphur donor ligands; the crystal and molecular structure of aqua[1,7-bis(N-methylbenzimidazol-2′-yl)-2,6-dithiaheptane]copper(II) perchlorate. *J. Chem. Soc., Dalton Trans.*, **1984**, 1349-1356.
48 Coe, B. J. & Glenwright, S. J. Trans-effects in octahedral transition metal complexes. *Coord. Chem. Rev.* **2000**, *203*, 5-80.
49 Lummiss, J. A. M., Higman, C. S., Fyson, D. L., McDonald, R. & Fogg, D. E. The divergent effects of strong NHC donation in catalysis. *Chem. Sci.* **2015**, *6*, 6739-6746.
50 Ru-O bond length decreases when less electron donating ligand are employed, e.g. Vougioukalakis, G. C. & Grubbs, R. H. Ruthenium-Based Olefin Metathesis Catalysts Coordinated with Unsymmetrical N-Heterocyclic Carbene Ligands: Synthesis, Structure, and Catalytic Activity. *Chem. Eur. J.* **2008**, *14*, 7545-7556.
51 Falivene, L. *et al.* Towards the online computer-aided design of catalytic pockets. *Nature Chem.* **2019**, *11*, 872-879.
52 César, V. *et al.* Ruthenium Catalysts Supported by Amino-Substituted N-Heterocyclic Carbene Ligands for Olefin Metathesis of Challenging Substrates. *Chem. Eur. J.* **2017**, *23*, 1950-1955.
53 Hunter, C. A. & Sanders, J. K. M. The nature of .pi.-.pi. interactions. *J. Am. Chem. Soc.* **1990**, *112*, 5525-5534.
54 Zhao, R. & Zhang, R.-Q. A new insight into π−π stacking involving remarkable orbital interactions. *Phys. Chem. Chem. Phys.* **2016**, *18*, 25452-25457.
55 Previous report featuring isolation and characterization of the decomposition product from BIPh ruthenium olefin metathesis catalyst focuses only on its PCy_3 derivative, ref. 23.
56 However, such loading is still considered low in the context of the challenging formation of C–C tetrasubstituted bonds, cf. Refs. 13-14.
57 Higman, C. S., Plais, L. & Fogg, D. E. Isomerization During Olefin Metathesis: An Assessment of Potential Catalyst Culprits. *ChemCatChem* **2013**, *5*, 3548-3551.
58 Krompiec, S. *et al.* The role of the functional group in double bond migration in allylic systems catalysed by ruthenium hydride complexes. *J. Mol. Catal. A Chem.* **2006**, *253*, 132-146.
59 Schmidt, B. Catalysis at the Interface of Ruthenium Carbene and Ruthenium Hydride Chemistry: Organometallic Aspects and Applications to Organic Synthesis. *Eur. J. Org. Chem.* **2004**, *2004*, 1865-1880.
60 Chatterjee, A. K., Sanders, D. P. & Grubbs, R. H. Synthesis of Symmetrical Trisubstituted Olefins by Cross Metathesis. *Org. Lett.* **2002**, *4*, 1939-1942.

61 Ablialimov, O., Kędziorek, M., Malińska, M., Woźniak, K. & Grela, K. Synthesis, Structure, and Catalytic Activity of New Ruthenium(II) Indenylidene Complexes Bearing Unsymmetrical N-Heterocyclic Carbenes. *Organometallics* **2014**, *33*, 2160-2171.
62 Debleds, O. & Campagne, J.-M. 1,5-Enyne Metathesis. *J. Am. Chem. Soc.* **2008**, *130*, 1562-1563.